Selective Diffusion of C8 Aromatics in a 10 and 12 MR Zeolite. A Molecular Dynamics Study

German Sastre,[†,‡] Nilesh Raj,[†] C. Richard A. Catlow,*[,†] Rolando Roque-Malherbe,[‡,#] and Avelino Corma[‡]

Davy Faraday Research Laboratory, The Royal Institution of Great Britain, 21 Albemarle Street, London W1X 4BS, U.K., and Instituto de Tecnologia Quimica, UPV−CSIC, Av/ Naranjos s/n; 46022 Valencia, Spain

Received: November 3, 1997

Molecular dynamics simulations employing a flexible framework are used to simulate the diffusion of *o*- and *p*-xylene in purely siliceous zeolite CIT-1. The simulations are performed at 500 K, investigating two loadings (corresponding to 1 molecule/unit cell and 0.25 molecule/unit cell) for the ortho isomer and one loading (0.25 molecule/unit cell) for the para isomer. For the former system the diffusion coefficient decreases from 7.79×10^{-6} cm^2/s for the lower to 3.56×10^{-6} cm^2/s for the higher loading. The diffusion coefficient for the para isomer (25.18×10^{-6} cm^2/s) is substantially greater. Graphical analyses reveal a jump diffusion mechanism, which in the case of the ortho isomer takes place in the 12 MR channels of the structure, while for the para isomer, incursions into the 10 MR channel are observed. The results of the MD simulations are complemented and reinforced by calculations of the activation energies for the diffusion of the two isomers in the two channels. Diffusivity measurements of both isomers in B-CIT-1 (Si/Al = 35) by FTIR have also been carried out in order to compare the values obtained theoretically and experimentally.

1. Introduction

The study of the diffusion of sorbates through the 3-D channel systems of zeolites has become increasingly important owing to the need to obtain a better understanding of the mechanisms of catalysis and adsorption in these materials. Although the crystallinity of zeolites provides good opportunities for explaining diffusivity of sorbed molecules in terms of structure−property relationships, many aspects of the mechanisms involved in the diffusion process remain unclear. Moreover, large differences (sometimes of several orders of magnitude) in diffusion coefficients obtained by different techniques[1] have commonly been one of the main obstacles to achieving a better understanding of diffusion in zeolites, where small changes in some of the variables of the system such as chemical composition, cation content, extraframework aluminum, crystallinity, temperature, and loading can lead to dramatic variations in the diffusivity of the guest molecules.[1−4]

Although, in some cases, the diffusional behavior of these systems can often be understood in a general way in terms of the relative size of the sorbate and the channel system,[5,6] such explanations have to be revised to explain phenomena such as "inverse shape selectivity" in which the formation of branched products is favored due to stabilizing interactions between the organic molecule and the walls of the zeolitic channel in hydrocracking reactions.[7] Predicting the balance between attractive and repulsive host−guest interactions while taking into account factors such as chemical composition and framework type is difficult owing to the large number of variables needed for a correct treatment of these phenomena and also to the frequent contradictions in the results obtained by different techniques. Moreover, both sorption and diffusion in zeolites may be investigated using computer modeling techniques.[8] On the other hand, experimental study of diffusion processes is reaching a turning point due to the existence of techniques in which the movement of the molecules is tracked directly. In particular methods such as PFG NMR (pulse field gradient nuclear magnetic resonance)[9] and QENS (Quasi-Elastic Neutron Scattering)[10] have provided reliable microscopic measurements of self-diffusivity.

The recent advances in computational chemistry and the advent of parallel computing have made possible much more realistic MD (molecular dynamic) studies. Atomistic simulations based on interatomic potentials have proved to be effective in modeling the diffusion of organic molecules in zeolites.[11−16] Although this approach has serious limitations in simulating chemisorption phenomena, which in most cases requires a quantum-chemical treatment, atomistic MD simulations provide an excellent method for simulating diffusion. We should emphasize that the simulation of purely diffusional processes is of major importance in providing a quantitative understanding of shape selective catalysis. In particular, diffusion constitutes an important step in zeolite catalysis as the sorbates have to travel through the channel systems before reaction occurs at the active site.[17]

It is known that the availability of numerous structural types in zeolites often permits the selection of the most appropriate structure to obtain the desired reaction products. Among the newly synthesized zeolites, CIT-1[18] represents a particularly interesting structure, for it is one of the first microporous materials with channel systems of 10 and 12 MR (membered rings). Both channel systems have been investigated in separate structures in studies of the diffusion of C6−C8 aromatics.[19−22] Such studies are particularly interesting as aromatic alkylation is one of the main applications of zeolites as catalysts. The

[†] The Royal Institution of Great Britain.
[‡] Instituto de Tecnolgia Quimica.
[#] Current address: Center for Theoretical Studies of Physical Systems, Clark-Atlanta University, Atlanta, GA 30314.

S1089-5647(98)00053-4 CCC: $15.00
Published on Web 04/07/1998

existence of both channel systems in the same structure represents a new challenge in the optimization of the industrial production of these compounds and in gaining new insights into the diffusional properties of hydrocarbons in zeolites.

In this paper, the study of the diffusion of *p*- and *o*-xylene in all-silica zeolite CIT-1 has been carried out by performing atomistic MD simulations. Additionally, diffusivity measurements of both isomers in B-CIT-1 (Si/Al = 35) by FTIR have been undertaken in order to compare the values obtained theoretically and experimentally. The aim of this work is to estimate the influence of the relative size of the two organic guest molecules on the diffusion coefficients and the influence of the channel system (12 and 10 MR) of the zeolite on the diffusion of each of the isomers. The results of our simulations improve our understanding of the influence of the relative size of zeolite pores and guest molecules on the diffusion coefficients.

2. Methodology

2.1. Molecular Dynamics Technique. Atomistic MD calculations have been performed to simulate the diffusion of *o*- and *p*-xylene in purely siliceous CIT-1. The calculations require the specification of a potential energy function which provides a description of the energy of the system as a function of nuclear coordinates and allows the calculation of its first derivatives from which the forces acting on each atom can be obtained. All the MD simulations have been carried out using the DL_POLY_2.0 program,[23] which is a general purpose MD code developed to run on a wide variety of computer architechtures, including workstations and MPP supercomputers. The parallel version is written in the replicated data form and uses standard message passing libraries as well as highly optimized hardware specific communications.

The simulation proceeds by first assigning initial velocities to all atoms according to a Maxwell−Boltzmann distribution which depends on the temperature of the system. From this starting point, Newton's equations of motion are solved using a finite time step by means of the standard Verlet algorithm.[24] Time steps of 1 fs and an equilibration temperature of 500 K have been employed in the present simulations. The zeolitic system comprises a 4 × 2 × 4 supercell of CIT-1 (SiO_2 composition) with a total of 2688 atoms to which parallelepiped periodic boundary conditions are applied. Different loadings of xylenes in the macrocell are modeled with the same periodic boundary conditions applied to the sorbates in the CIT-1 macrocell. The geometry of the zeolite is first optimized at 0 K using the BFGS[25] technique implemented in the GULP[26] code, and the result is used as input for a 25 ps equilibration stage of the zeolite + sorbate system. A "cap forces" directive (limited to 1000 kT/Å) avoids the collision between the atoms of the system, by precluding the possibility of any two atoms becoming too close after the assignment of the Maxwell−Boltzmann velocity distribution to all the atoms in the initial configuration. If the repulsive force between any two atoms becomes higher than the limiting value (in our case 1000 kT/Å), the program automatically freezes the coordinates of the atoms, avoiding the collision. This option was removed after being used in the initialization period of the simulation, after which the velocity rescaling algorithm is also removed and a run of 10 ps is performed to ensure that the temperature remains constant at 500 K within a fluctuation of ±3 K. After this period, runs of 100 ps were carried out within the NVE ensemble at 500 K; owing to the small temperature fluctuations, the results are equivalent to those that would have been obtained with the NVT ensemble at this temperature. The xylene loadings were 32 and 8 molecules in the CIT-1 macrocell, which corresponds to 1 and 0.25 molecule/unit cell, respectively. In all the simulations every atom was allowed to move explicitly, giving a total of 3264 and 2832 periodic atoms in the 1 and 0.25 molecule/unit cell cases, respectively.

We emphasize that full motion of the framework atoms has been considered throughout the simulations. Although this increases substantially the computational expense, the influence of the framework flexibility has been made clear in a number of studies.[12,15,27] This task has been successfully undertaken by the DL_POLY code in its fully parallelized implementation on a 512 PE CRAY-T3D MPP computer at the Edinburgh Parallel Computing Centre. The present simulations were mainly run using 128 processors.

During the simulation, history files were saved every 1000 steps; and subsequent analysis used the MSD facility included in DL_POLY to obtain mean square displacements. The expression used to calculate the MSD plots was the following:[28]

$$\langle X^2(t)\rangle = 1/(N_m N_{to}) \sum_{to} \sum_{i} [X_i(t + t_0) - X_i(t_0)]^2 \qquad (1)$$

where N_m is the number of diffusing molecules, N_{to} is the number of time origins used in calculating the average, and X_i is the coordinate of the center of mass of molecule i.

The diffusion coefficients are then calculated using the Einstein relation

$$\langle X^2(t)\rangle = 6Dt + B \qquad (2)$$

where t is the simulation time, and B is the thermal factor arising from atomic vibrations.

2.2. Interatomic Potentials. Four types of interatomic potentials are needed to model this system:

$$V_{total} = V_{zeolite} + V_{xylene} + V_{xylene-xylene} + V_{zeolite-xylene} \qquad (3)$$

The potential for the framework, $V_{zeolite}$, was originally derived by Catlow et al.[13] and is essentially a Born model potential comprising three terms:

$$V_{zeolite} = V_{buck} + V_{three-body} + V_{coul} \qquad (4)$$

The first is a short-range, polynomial, four-range Buckingham splined function (see Table 1) for which a cutoff distance of 7.6 Å was used. A three-body, O−Si−O, nonharmonic potential was chosen to describe bond angle-bending forces. Finally, the long-range electrostatic interactions were calculated by means of the Ewald summation technique using formal charges.

The potential for the sorbate, V_{xylene}, comprises four terms and was taken from Oie et al.:[29]

$$V_{xylene} = V_{two-body} + V_{three-body} + V_{four-body} + V_{coul} \qquad (5)$$

Four different atom types are considered in the xylene molecule: CA, CB, HA, HB, the atoms labeled A belonging to the aromatic ring and those marked B forming part of the methyl groups. All appropriate two-body, three-body, bond-bending, and four-body (i.e. dihedral angle torsional terms) terms are included; details are given in Table 2, which also reports the partial charges used for the different atoms; the latter were taken from Auerbach et al.[30]

Finally, 12−6 Lennard-Jones potentials and Coulombic interactions (with the charges already mentioned) were used to

TABLE 1: Potential Form for the All-Silica Zeolite

$V_{zeolite} = V_{buck} + V_{three-body} + V_{coul}$ (eq 4)[a]

$V_{buck} = A_{ij} \exp(-r_{ij}/\rho_{ij})$ $r_{ij} < r_1$

$V_{buck} = B_{ij}(r_{ij})^5 + C_{ij}(r_{ij})^4 + D_{ij}(r_{ij})^3 + E_{ij}(r_{ij})^2 + F_{ij}r_{ij} + G_{ij}$ $r_1 < r_{ij} < r_2$

$V_{buck} = H_{ij}(r_{ij})^3 + I_{ij}(r_{ij})^2 + J_{ij}r_{ij} + K_{ij}$ $r_2 < r_{ij} < r_3$

$V_{buck} = -L_{ij}/(r_{ij})^6$ $r_3 < r_{ij} < r_c$

$V_{three-body} = (1/4)A_{ijk}(B_{ijk})^2 \exp(-r_{ij}/\lambda) \exp(-r_{ik}/\lambda)$

where $A_{ijk} = (1/2)K_{ijk}(\theta_0 - \pi)^2$;

$B_{ijk} = (\theta_0 - \pi)^2 - (\theta - \pi)^2$

$V_{coul} = q_i q_j / r_{ij}$ where $q(O) = -2.0$; $q(Si) = +4.0$

parameter	Si−O	O−O
r_1 (Å)	1.5	2.9
r_2 (Å)	2.5	3.6
r_3 (Å)	3.5	4.2
r_c (Å)	7.6	7.6

[a] The short-range Buckingham potential for Si−O and O−O interactions is a function splined at r_1, r_2, and r_3 to have continuous first and second derivatives, and a minimum at r_2. A cutoff distance r_c = 7.4 Å was employed in the MD simulations.

TABLE 2: Potential Form and Parameters Used for *o*- and *p*-xylene Molecules

$V_{xylene} = V_{two-body} + V_{three-body} + V_{four-body} + V_{coul}$ (eq 5)

$V_{two-body} = (1/2)k_{ij}(r_{ij} - r_{ij}^0)^2$

$V_{three-body} = (1/2)k_{ijk}(\theta_{ijk} - \theta_{ijk}^0)^2$

$V_{four-body} = A_{ijkl}[1 + \cos(n\phi_{ijk} - \delta_{ijkl})]$

$V_{coul} = q_i q_j / r_{ij}$ where $q(CA) = -0.153$; $q(CB) = +0.483$; $q(HA) = +0.153$; $q(HB) = -0.110$

two-body parameters	k_{ij} (eV Å^{-2})	r_{ij}^0 (Å)
CA−CA	48.94	1.385
CA−CB	31.75	1.510
CA−HA	31.25	1.085
CB−HB	28.75	1.095

three-body parameters	k_{ijk} (eV)	θ_{ijk}^0 (deg)
CA−CA−CA	3.44	120.0
CA−CA−CB	3.44	120.0
CA−CA−HA	3.44	120.0
CA−CB−HB	2.50	109.5
HB−CB−HB	2.06	109.5

four-body parameters	A_{ijkl} (eV)	n	δ_{ijkl} (deg)
CA−CA−CA−CA	0.2166	2.0	180.0
CA−CA−CA−HA	0.0867	2.0	180.0
CA−CA−CA−CB	0.0867	2.0	180.0
CB−CA−CA−HA	0.0867	2.0	180.0
HA−CA−CA−HA	0.0867	2.0	180.0
CA−CA−CB−HB	0.0043	3.0	0.0

describe the guest−guest and framework−guest, atom−atom interactions according to the following equations:

$$V_{xylene-xylene} = V_{Lennard-Jones} + V_{coul} \quad (6)$$

$$V_{zeolite-xylene} = V_{Lennard-Jones} + V_{coul} \quad (7)$$

All guest−guest and framework−guest interactions are reported in Table 3 and were taken from ref 13, in which the guest molecule considered is benzene. In the $V_{xylene-xylene}$ and $V_{zeolite-xylene}$ potentials, additional terms had to be included in the summation to take into account interactions due to the substituent methyl groups in the aromatic ring.

3. Experimental Section

3.1 Materials. Zeolite B-CIT-1 was kindly provided by M. E. Davis.[18] The crystallinity of the solid was determined using X-ray powder diffraction (Cu Kα radiation), and the measurements were done with a Phillips diffractometer model PW 1710, equipped with a graphite monochromator and scintillation counter. The results indicated that the crystallinity of the sample was close to 100%.

TABLE 3: Potential Parameters Used for Xylene−Xylene and Zeolite−Xylene Interactions

$V_{xylene-xylene} = V_{Lennard-Jones} + V_{coul}$ (eq 6)

$V_{zeolite-xylene} = V_{Lennard-Jones} + V_{coul}$ (eq 7)

$V_{xylene-xylene} = (A_{ij}/r_{ij})^{12} - (B_{ij}/r_{ij})^6$

$V_{zeolite-xylene} = (A_{ij}/r_{ij})^{12} - (B_{ij}/r_{ij})^6$

Lennard-Jones parameters	A_{ij} (eV Å^{12})	B_{ij} (eV Å^6)
CA−CA	32 475.0	29.838
CA−CB	32 475.0	29.838
CB−CB	19 692.0	18.0933
CA−HA	3721.2	7.6182
CA−HB	3721.2	7.6182
CB−HA	2800.0	5.8415
CB−HB	2800.0	5. 8415
HA−HA	384.840	1.9867
HA−HB	384.840	1.9867
HB−HB	384.840	1.9867
CA−O	15 000.0	22.402
CB−O	11 000.0	17.654
HA−O	1556.4	5.5717
HB−O	1556.4	5.5717

Scanning electron microscopy (JEOL-ISM 6300) of the sample was carried out to determine the crystal size and morphology of the CIT-1 zeolite. Spherical shaped crystals were found with an average diameter of 1.5 mm. For the removal of tetrahedral framework boron and insertion of aluminum in B−CIT-1, the corresponding calcined borosilicate was exchanged with 2% (w/w) water solution of $Al(NO_3)_3$ at 100 °C and a sample of H−Al−CIT-1 (H−CIT-1) was produced. Atomic absorption spectroscopy (Varian SpectrAA 10 Plus spectrophotometer) was used for the determination of the chemical composition of the sample. The analyses gave a bulk Si/Al ratio of 35 for H−CIT-1. *o*-xylene and *p*-xylene (Aldrich) were all analytical grade reagents and were further dehydrated using zeolite 4A.

3.2. Experimental Procedure. Measurement of the sorption kinetics with the FTIR (BIORAD FTS 40A) method[21] was carried out by monitoring the change in the integrated intensity (absorbance) of the IR typical bands of the sorbate molecules, i.e. *o*-xylene and *p*-xylene.[19,31] The diffusion experiments were carried out in a water-cooled AABSPEC IR cell, which, as previously described,[19] allows us to work up to 700 K. The windows are made of CaF_2, and the temperature of the sample holder is controlled electronically with 1 °C of precision. The complete experimental setup is composed of the IR cell connected through stainless steel pipes to a manifold which contains two thermostatically controlled saturators and was previously described in detail.[19,31] Self-supported wafers, obtained by pressing 10−12 mg/cm^2 of the zeolite sample powder at 400 MPa, were placed in the cell sample holder. These wafers ensure that there are no macroporous limitations for the transport of the hydrocarbon molecules during the sorption process, so that it is possible to measure intracrystalline diffusion.

Prior to the measurement of diffusivities, the samples were carefully dehydrated at 673 K for a period of 2 h in a flow of nitrogen. After activation, the sample was cooled to the desired temperature and kept at this temperature with the help of a thermostat. The flow rates were adjusted to get the desired relative partial pressure. A background spectrum of the pure

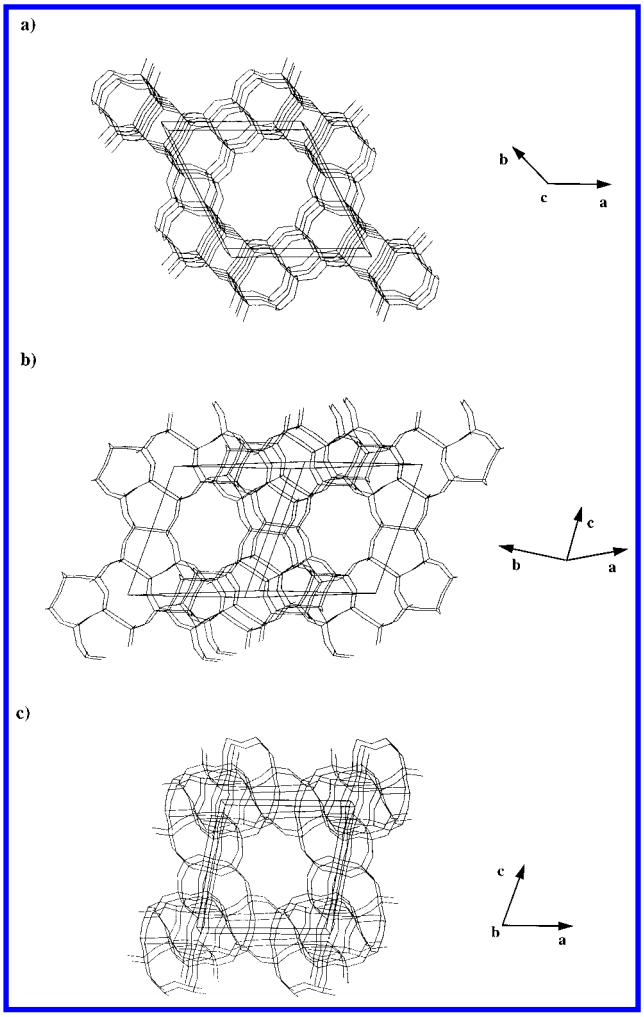

Figure 1. CIT-1 macrocell optimized at 0 K. Projections along (a) [001] (12 MR); (b) [110] (10 MR); (c) [010] (12 MR).

degassed zeolite was obtained as a reference.[19,21] The transport diffusion coefficients were calculated with the solution of Fick's second law:[31]

$$M_t/M_\infty = 1 - (3D_e/ba^2)e^{-bt}\{1 - (\ddot{O}ba^2D_e)\cot(\ddot{O}ba^2D)\} + (6ba^2/D_ep^2)S\{\exp(-D_en^2p^2t/a^2)/[n^2(n^2p^2 - ba^2/D_e)]\} \quad (8)$$

where M_t (proportional to the absorbance A_t) is the amount of sorbate at time t, M_∞ is the equilibrium sorption value (proportional to A_∞), D is the Fickean diffusion coefficient, a is the radius of the zeolite crystallite, and b is a time constant that describes the evolution of the sorptive partial pressure in the dead space of the IR cell: $P = P_0(1 - \exp(-bt))$, P being the pressure at time t.

The use of eq 8 is justified when diffusion occurs in uniform spherical particles of radius, a,[17] as is the case for the diffusion in the H−CIT-1 zeolite, where we have spherical shape crystals with $a = 0.75$ mm.

4. CIT-1 Diffusional Network

As has been noted in section 1, CIT-1 (IZA coded CON) is a zeolite containing channel systems with 10 and 12 MR, the 12 MR channels being parallel to [001] and [010] and the 10 MR channels being parallel to [110] (Figure 1). In their original paper Lobo et al.[18] describe the structure in the *C*2/*m* crystallographic space group. In this study we have found that the optimized 0 K structure lowers the symmetry to a triclinic cell with parameters, $a = b = 13.0868$ Å, $c = 12.3494$ Å, $\alpha = 107.579°$, $\beta = 72.491°$, $\gamma = 118.308°$. Such reductions in symmetry have previously been found in computer simulations of microporous materials such as $AlPO_4$-5.[32] We should stress that reducing the symmetry of the original system does not involve a substantial change in the coordinates of the atoms of the unit cell. The optimized unit cell of CIT-1 contains 84 atoms (28 Si and 56 O).

In this study we make extensive use of visualization of trajectories of the centers of mass of the sorbate molecules, to elucidate the diffusion process in the different channel systems. The MD simulations give, as output, a history file with the Cartesian coordinates of all the atoms of the system as a function of time. To visualize the history files, we generate two kind of graphics: first, *history graphs* are derived in order to reveal how the *x*, *y*, *z* coordinates vary with simulation time; second, *trajectory graphs* corresponding to "*x* vs *y*", "*x* vs *z*", and "*y* vs *z*" are shown in order to visualize the diffusion path. To understand the diffusion path with respect to the zeolite channel system, we project both the channels and the sorbate path onto the two-dimensional planes mentioned. By this procedure, the channel(s) through which each molecule is diffusing can be visualized. In the "trajectory graphs" each of the channels is represented by a straight line corresponding to the coordinates of the axis of the channel. All the 12 MR channels are parallel in each graph, as are the 10 MR channels. Each channel system is then characterized by its slope, which is calculated from the crystallographic parameters and the crystallographic channel direction.

The *trajectory graphs* contain all the visual information needed to understand, at first sight, the basic mechanism of the diffusion process; in particular they allow us to see which molecules are diffusing through which channels. Although both channel systems appear clearly differentiated in all three trajectory graphs and each gives almost all the information needed, the close inspection of all three perspectives is needed to achieve a complete and coherent understanding of the diffusion process.

5. Results and Discussion

5.1. Molecular Dynamics Simulations. The 4 × 2 × 4 CIT-1 macrocell is shown in Figure 1. We recall that before undertaking the MD simulation we optimized the structure starting from the reported coordinates. As noted in section 3, the optimization gives a lower symmetry, triclinic system that, however, has very similar atomic coordinates, bond lengths, and bond angles. The channel dimensions after the 0 K optimization, i.e. 7.0 × 6.6 Å and 5.3 × 5.5 Å for the 12 and 10 MR channel systems, respectively, are also very close to previously reported values.[18]

Previous studies have shown how the pore dimension in zeolites may vary due to the framework flexibility.[33] A run of 10 ps was performed to study this effect in CIT-1, for which a temperature of 200 K was chosen. The results show little variations in the geometry of the 12 MR channels but found a significant change in the 10 MR dimensions, which ranged during the run from 6.5 × 5.2 Å to 5.2 × 6.5 Å (compared with 5.3 × 5.5 Å in the 0 K energy minimized structure). Figure 2 shows this effect more clearly. Detailed analysis and further simulations are currently in progress to determine how this effect varies with temperature.

With the optimized 0 K structure as the initial conformation, the xylene molecules were introduced into the framework. In

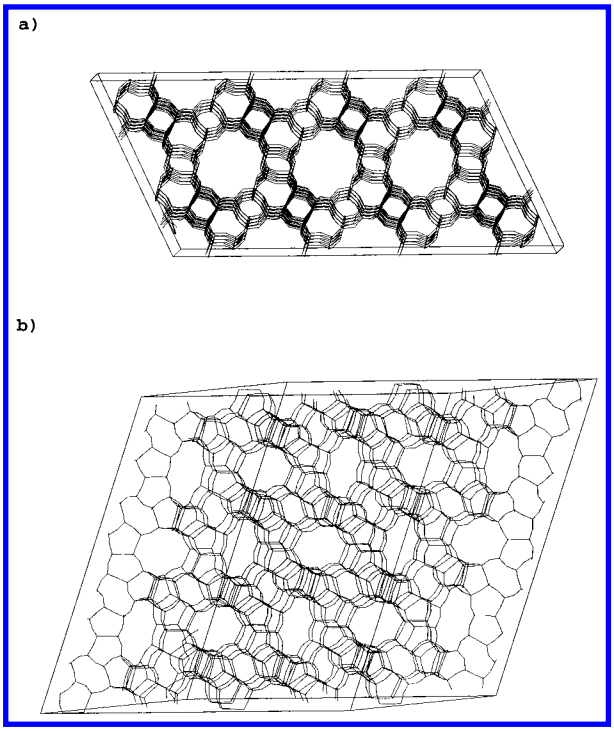

Figure 2. 4 × 2 × 4 CIT-1 macrocell after a 10 ps run at 200 K. Projections along (a) [001]; (b) [110]. The latter shows the change in the 10 MR pore shape (paralell to [110]) with respect to those in Figure 1. The pore shapes along [001] and [010] remain the same in both cases.

the first simulation, 32 *o*-xylene molecules are located in the zeolite framework, giving an average loading of 1 molecule/unit cell. The results from the MD simulation on this system yield the MSD plot shown in Figure 3a. The diffusion coefficient obtained from the MSD plot (3.56×10^{-6} cm^2/s, in Table 4) indicates that the molecules are not locked within the channel systems but rather show appreciable diffusion through the structure. The absence of cations in the structure allows the *o*-xylene molecules to diffuse with no restriction other than those due to the channel size and xylene−xylene interactions. The trajectory plots in Figure 4 show the motion of the 32 *o*-xylene molecules through the channel systems of CIT-1. Two main features are evident from this figure. The first is that the 32 *o*-xylene molecules diffuse through the 12 MR channel system, which explains the relatively high calculated diffusion coefficient, which is comparable to that obtained by MD simulations of diffusion in 12 MR zeolites such as β and Y. The simulations occasionally show some attempts to enter the 10 MR channels, but after penetrating the opening of the 10 MR channels the *o*-xylene molecules go back to the 12 MR, where the diffusion process is more favorable. The second feature is that the motion of the *o*-xylenes is relatively hindered even in the 12 MR channels, as can be seen from the history plots (Figure 5) in which the *x*,*y*,*z* coordinates remain steady for long periods of time through the 100 ps run and then change rapidly, indicating a jump diffusion mechanism. All the jumps correspond to diffusion through 12 MR channels. The *o*-xylene molecules spend a considerable amount of time of the simulation diffusing in the restricted parts of the CIT-1 structure corresponding to the intersection between the 12 MR and 10 MR channels, in what we call "extensive local motion".

To estimate the effect of xylene−xylene interactions on the mobility of the *o*-xylene molecules, a second simulation was performed at lower loading. In this case, 8 *o*-xylene molecules were distributed in the CIT-1 macrocell, which corresponds to

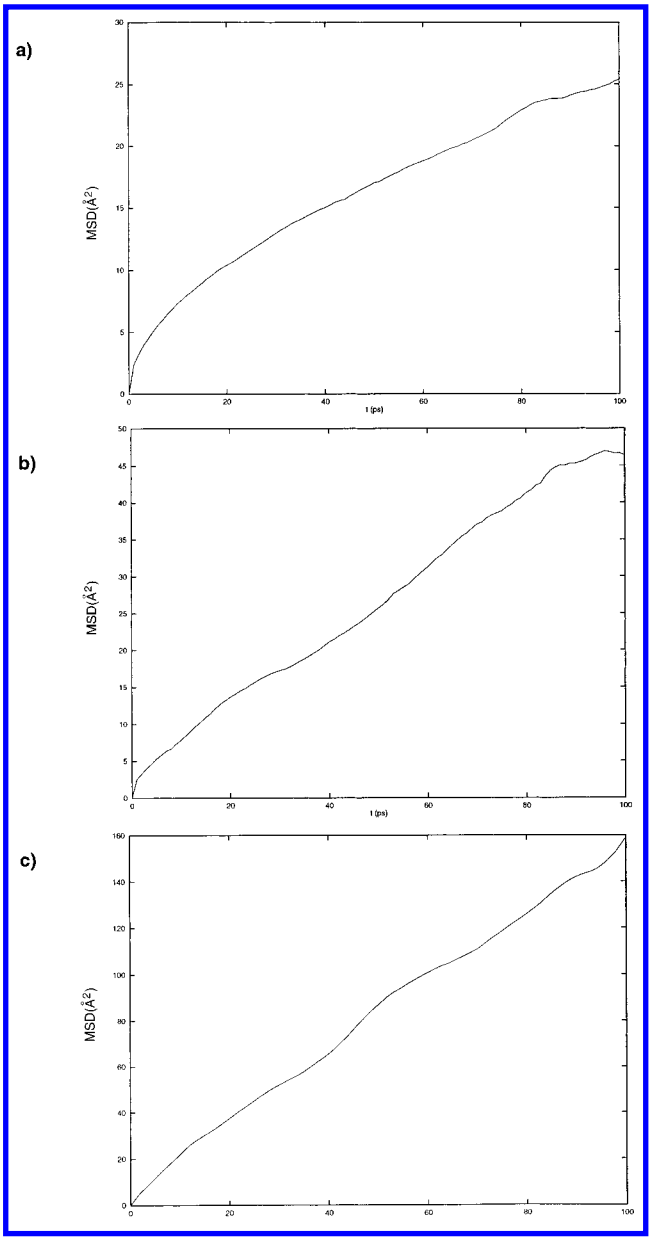

Figure 3. MSD plots for the different loadings of the 4 × 2 × 4 CIT-1 macrocell: (a) 32 *o*-xylene molecules; (b) 8 *o*-xylene molecules; (c) 8 *p*-xylene molecules.

TABLE 4: Diffusion Coefficients Obtained from the MSD Plots in Figure 3

xylene loading in the 4 × 2 × 4 CIT−1 macrocell	diffusion coefficient (cm^2/s)
32 *o*-xylenes	3.56×10^{-6}
8 *o*-xylenes	7.79×10^{-6}
8 *p*-xylenes	25.18×10^{-6}

an average loading of 0.25 molecule/unit cell. The MSD plot (Figure 3b) shows clear differences with respect to the previous case. The diffusion is now markedly faster, as indicated by the higher diffusion coefficient of 7.79×10^{-6} cm^2/s (Table 4). Xylene−xylene interactions are much less important when the loading is 0.25 molecule/unit cell, with the diffusion controlled by molecule−host interactions. Two kinds of trends in the variation of diffusion with loading at low loadings are traditionally observed in zeolites. In some cases the diffusion at very low loading is small because the first molecules are adsorbed in pockets, allowing the subsequent molecules to diffuse faster. In other cases when pockets are not present in

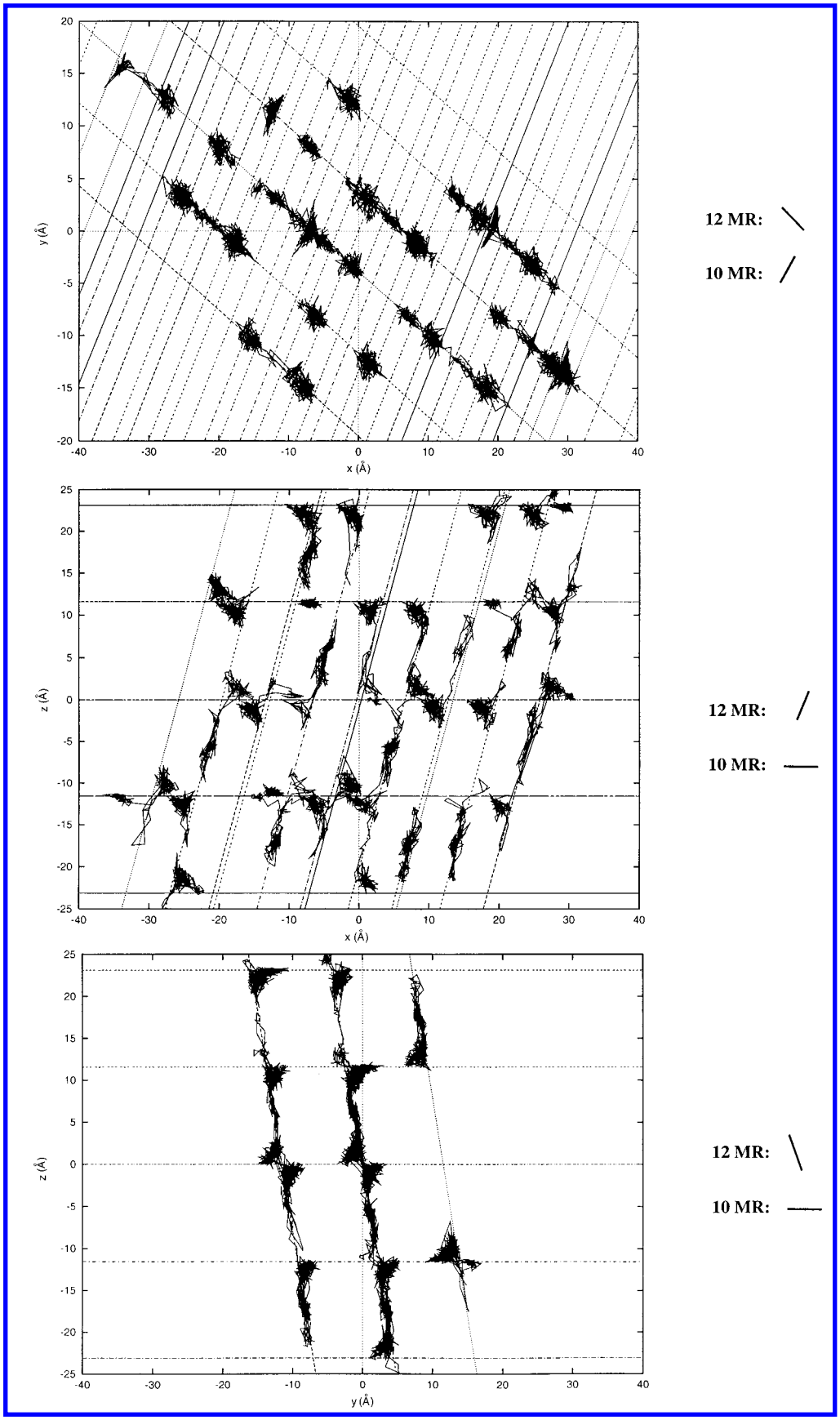

Figure 4. Trajectory plots "*x* vs *y*", "*x* vs *z*", and "*y* vs *z*", for the loading of 32 *o*-xylene molecules. The diagrams show the diffusion path of the center of mass of the sorbate molecules. (The channels are represented as straight lines).

the structure, interference between the molecules results in a decrease in the diffusivity over the entire range of loading. CIT-1 seems to behave in the latter manner. The results obtained with 0.25 and 1.0 molecules/unit cell loading show that the diffusion coefficients decrease with loading. Simulations over a wider range of loading would be needed to confirm that this trend

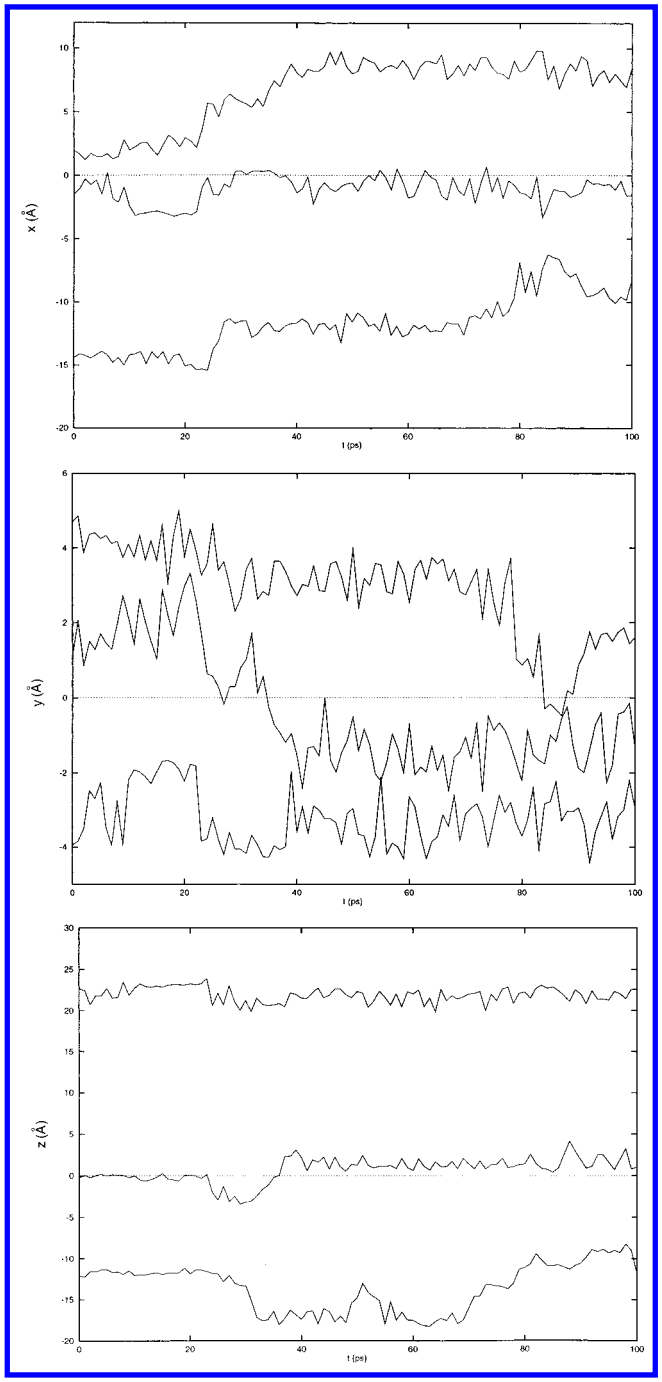

Figure 5. History plots "*x* vs *t*", "*y* vs *t*", and "*z* vs *t*", for the loading of 32 *o*-xylene molecules. To simplify the diagram, only the coordinates of four molecules have been plotted

persists at different loadings. The trajectory plots for the system with lower loading (Figure 6) are similar to these with the higher loading, reinforcing our earlier conclusions regarding the extensive local motion in the *o*-xylene trajectories due to the relatively large size of the *o*-xylene with respect to the channels. The diffusion in the system with lower loading occurs also through the 12 MR channels, as illustrated by the trajectory plot in Figure 7, although the same frustrated attempts to penetrate the 10 MR channels are observed (Figure 6). These attempts will occur with higher probability at very high loading when saturation of the 12 MR could force *o*-xylene toward the 10 MR channels. Diffusion in the narrower channels will not occur due to the high activation energy involved in this process. We can only expect to see diffusion through the 10 MR channels at very high loading when saturation of the 12 MR forces *o*-xylene into the narrower pores, a point to which we return below.

To estimate the effect of the shape of the sorbate molecules on the diffusion, a simulation with 8 *p*-xylene molecules in the CIT-1 macrocell was performed. It is well-known that, although the sizes of the ortho and para isomers are very similar, only *p*-xylene can diffuse through 10 MR channels, in particular those of ZSM-5.[34,35] The calculated diffusion coefficient, 25.18×10^{-6} cm^2/s, obtained from the MSD plot (Figure 3c), is much higher than for the simulation with 8 *o*-xylenes (Table 4). The higher mobility of the *p*-xylene molecules can clearly be seen from the history plots (Figure 8), when these are compared with the corresponding plots for *o*-xylene (Figure 5). The molecules diffuse through a wider region of the framework in this case. The trajectory plots (Figure 9) show that the diffusion occurs mainly through the 12 MR channels, but some incursions into the 10 MR channels are also observed. Although diffusion through the 12 MR channels is favored, and these channels are far from being saturated (with a loading of only 0.25 molecule/unit cell), some diffusion occurs also through the 10 MR channels. However, as we will show later, the activation energies for diffusion in the two channel systems are similar. Nevertheless, diffusion through the 10 MR system is much more restricted than in the 12 MR, and the incursions into 10 MR channels are shorter. It is also interesting to note that diffusion through the 10 MR channels precludes rotation of the *p*-xylene molecules because the size of the sorbate matches the channel dimensions. This inability of *p*-xylene to rotate decreases the time spent in this channel system.

At a loading of 0.25 molecule/unit cell, entrance into 10 MR channels is easy, as these channels are almost void, and exit is also easy, as 12 MR channels are far from being filled and probability of blockage is low. A different situation can be envisaged when the *p*-xylene loading is increased. In this case, the larger number of *p*-xylene molecules, initially present in the 12 MR channels, will make diffusion through these channels more difficult, which will increase the probability of diffusion through 10 MR channels. Exit from 10 MR channels will be more difficult due to high loading into 12 MR channels. An equilibrium between molecules in 12 and 10 MR will be eventually reached with the proportion of molecules in 10 MR being higher when the loading increases. A similar argument suggests a different result for the case of the *o*-xylene sorbate, for which diffusion through 10 MR channels is very unlikely due to relative shape effects and where no competitive diffusion through the channels is expected at any loading. Subsequent work will examine the behavior of a mixed *o*- and *p*-xylene sorbate system, which presents an interesting challenge for simulation, as the properties of mixed sorbates are still poorly understood.

Finally, a series of simulations were performed to estimate the relative activation energies for the diffusion of *o*- and *p*-xylene in the 12 and 10 MR channels. Here, a different methodology was used, employing the "solids diffusion path" facility implemented in the Catalysis6.0 software package of MSI.[36] The strategy followed consists of drawing the xylene molecule through a channel axis in steps of 0.2 Å, optimizing the position of the molecule at each step, and then calculating the energy. The result is a two-dimensional plot of energy versus channel coordinate that has a periodic form as a consequence of the periodicity of the structure. The calculations use a block of atoms of CIT-1 in its optimized 0 K geometry. The coordinates of the 2688-atom block corresponding to 4 ×

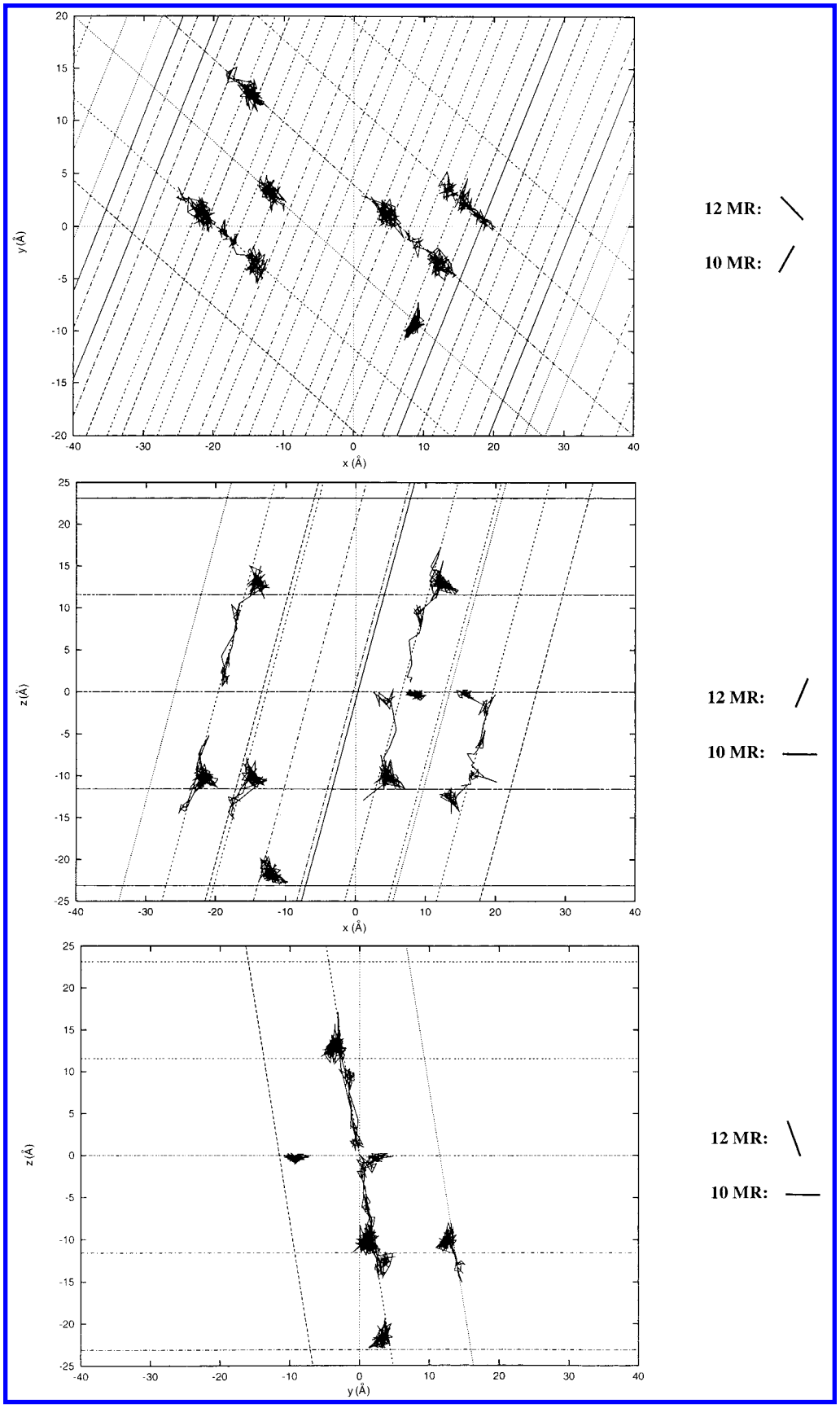

Figure 6. Trajectory plots for the loading of 8 *o*-xylene molecules.

2×4 unit cells of CIT-1 were kept fixed during the calculation. This approximation may be too restrictive, as framework dynamics in the MD simulation play an important role in the diffusion of sorbates especially when the size of the guest molecule and the channels are comparable. The effect of the use of a finite block rather than a periodic array is, however, not too important here because van der Waals interactions will be dominant and they are well taken into account by the zeolite

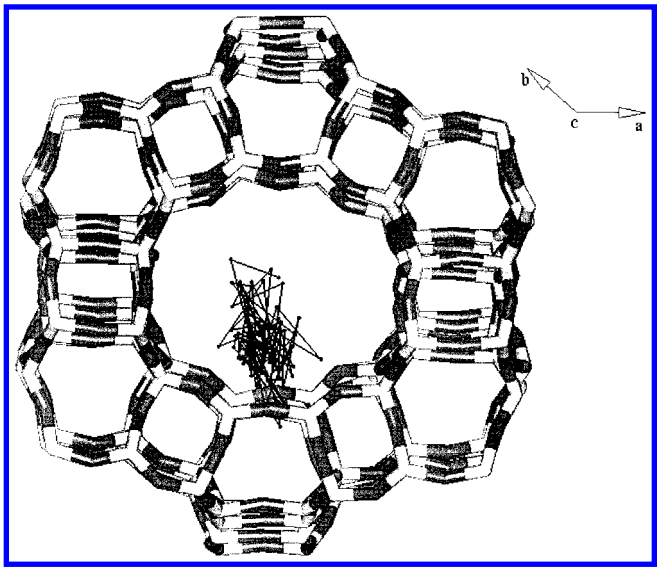

Figure 7. Trajectory of the center of mass of one of the *o*-xylene molecules (higher loading) in the 100 ps run showing diffusion through the 12 MR channel—perpendicular to the plane of the drawing—in purely siliceous CIT-1.

atoms located in the proximity of the diffusing sorbate. It should also be stressed that sorbate−sorbate interactions are not included in this treatment as only a single sorbate molecule is included in the simulation. The force field used in this study is taken from BIOSYM/MSI Catalysis6.0 software suite[36] and is different from that used in the MD work. For this reason, the results obtained for these simulations cannot be compared directly with results obtained from MD simulations nor do they provide an accurate estimation of the activation energy of the diffusion process. The results, however, allow us to obtain relative activation energies.

The resulting energy profiles are shown in Figure 10. The calculated activation energies, of 20.9 and 6.2 kcal/mol for *p*-xylene in 10 MR and 12 MR channels, respectively (see Table 5, Figure 10a, and Figure 10b), help to explain the selective diffusion through the 12 MR. As for the *o*-xylene diffusing through a 10 MR channel (Figure 10d), a very high activation energy—110.3 kcal/mol—is obtained. This precludes the possibility of this molecule diffusing through the smaller channels. No restriction seems to exist for the diffusion of *o*-xylene through 12 MR channels (Figure 10c) because the activation energy in this case is 7.0 kcal/mol. It is interesting to note that the activation energy through the 12 MR channels for both isomers is very similar. This result, however, does not imply a close similarity between the overall diffusion coefficients of the *o*-xylene and *p*-xylene since *p*-xylene also diffuses through the 10 MR channels. Nevertheless, the calculation shows that if the diffusion coefficients through the 12 MR channels alone were obtained, they should be very similar. The diffusion path of the *o*-xylene in the 12 MR channels also indicates that rotation of the sorbate is strongly restrained (except at the intersection of the channels), as is indicated in Figure 10c by the energy peak owing to an unoptimized orientation of the *o*-xylene molecule in the channel.

5.2. Experimental Measurements of Diffusivity. In Tables 6and 7, we give the experimental diffusion coefficients of *p*- and *o*-xylene and the activation energies for these processes. From these results and the Arrhenius equation the diffusion coefficients were calculated at 500 K and the values obtained are on the order of 10^{-9} cm^2/s, which are 3 orders of magnitude lower than those found in the MD simulations. This discrepancy might cast doubt on the procedures for data collection and analysis, but the values previously reported (as summarized in Table 8) for the diffusion of benzene, toluene, and xylenes in 10 and 12 MR zeolites, using ZLC[37−39] and FTIR[19,21] methods, indicate that the diffusion coefficients are of the same order as the values obtained here and are considerably below 10^{-6} cm^2/s. It is also interesting to note that the experimental activation energy for *p*-xylene is somewhat higher than that calculated for the isomer in the 12 MR channel, but lower than the calculated value for the 10 MR. This result may suggest that, as expected, the isomer is diffusing through both channels. The value calculated for the *o*-xylene diffusion in the 12 MR is substantially lower than the experimental value. Again, the occurrence of some diffusion in the 10 MR, which is likely at the high loadings used in the experimental work, may explain this difference. Contributions

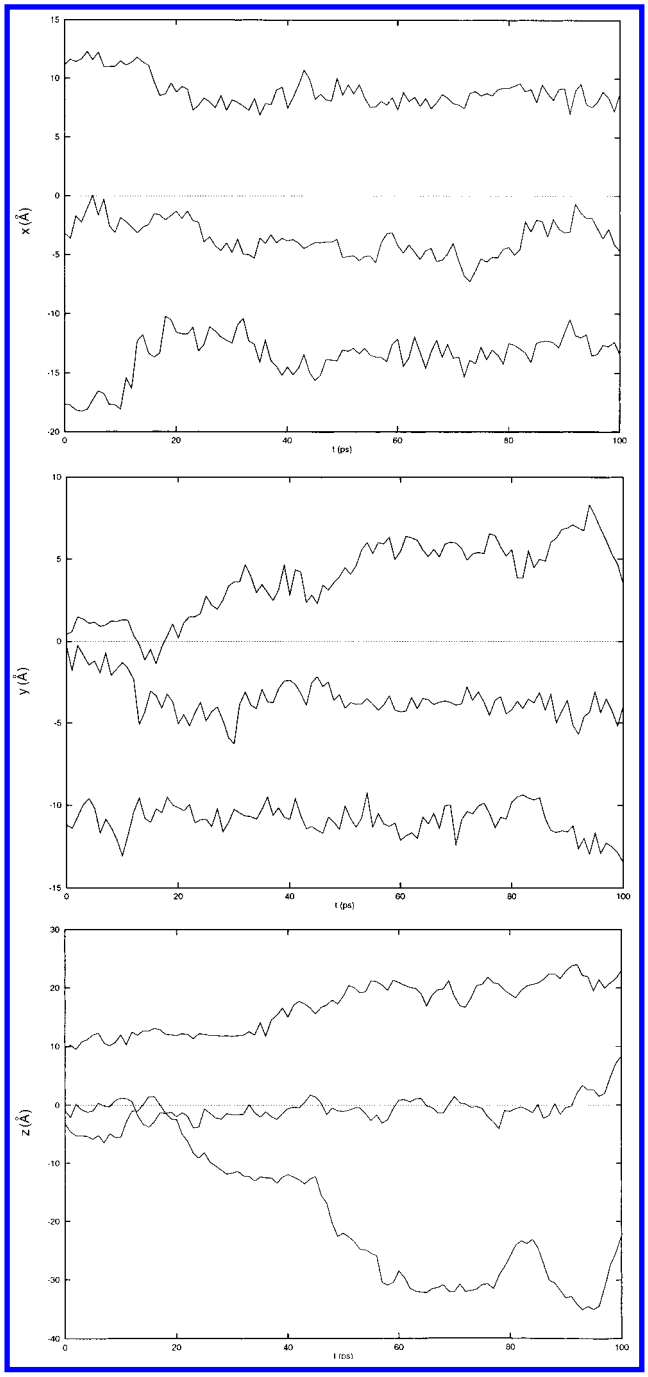

Figure 8. History plots for the loading of 8 *p*-xylene molecules.

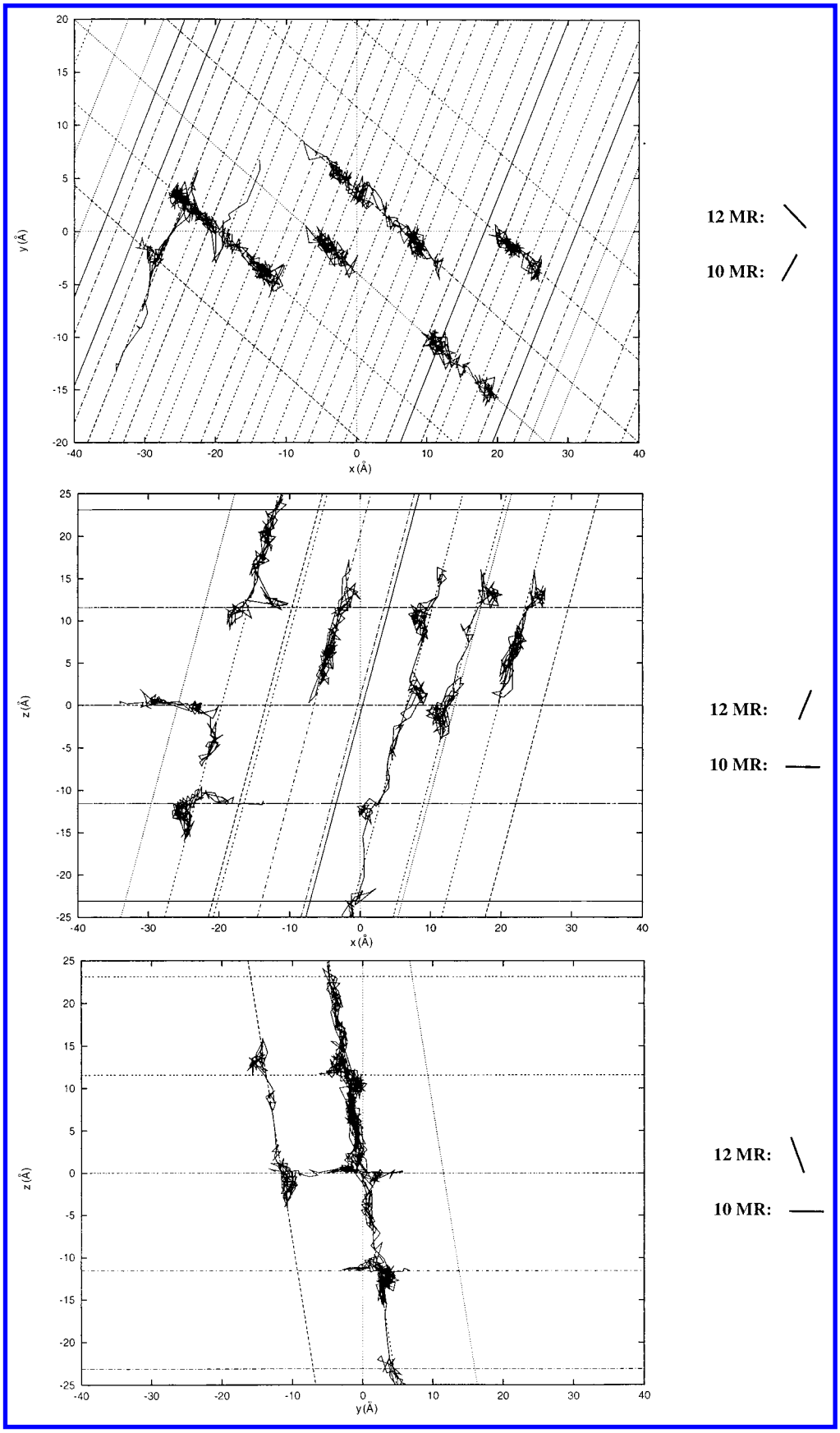

Figure 9. Trajectory plots for the loading of 8 *p*-xylene molecules.

from sorbate−sorbate interaction to the measured activation may also be appreciable.

The differences between the MD and experimental diffusion coefficients could arise from the fact that the simulations have modeled a purely siliceous zeolite while the experiments have been carried out with a zeolite with Si/Al = 35. To review the effects of these differences in chemical composition, it is instructive to consider previously reported data for ZSM-5 and

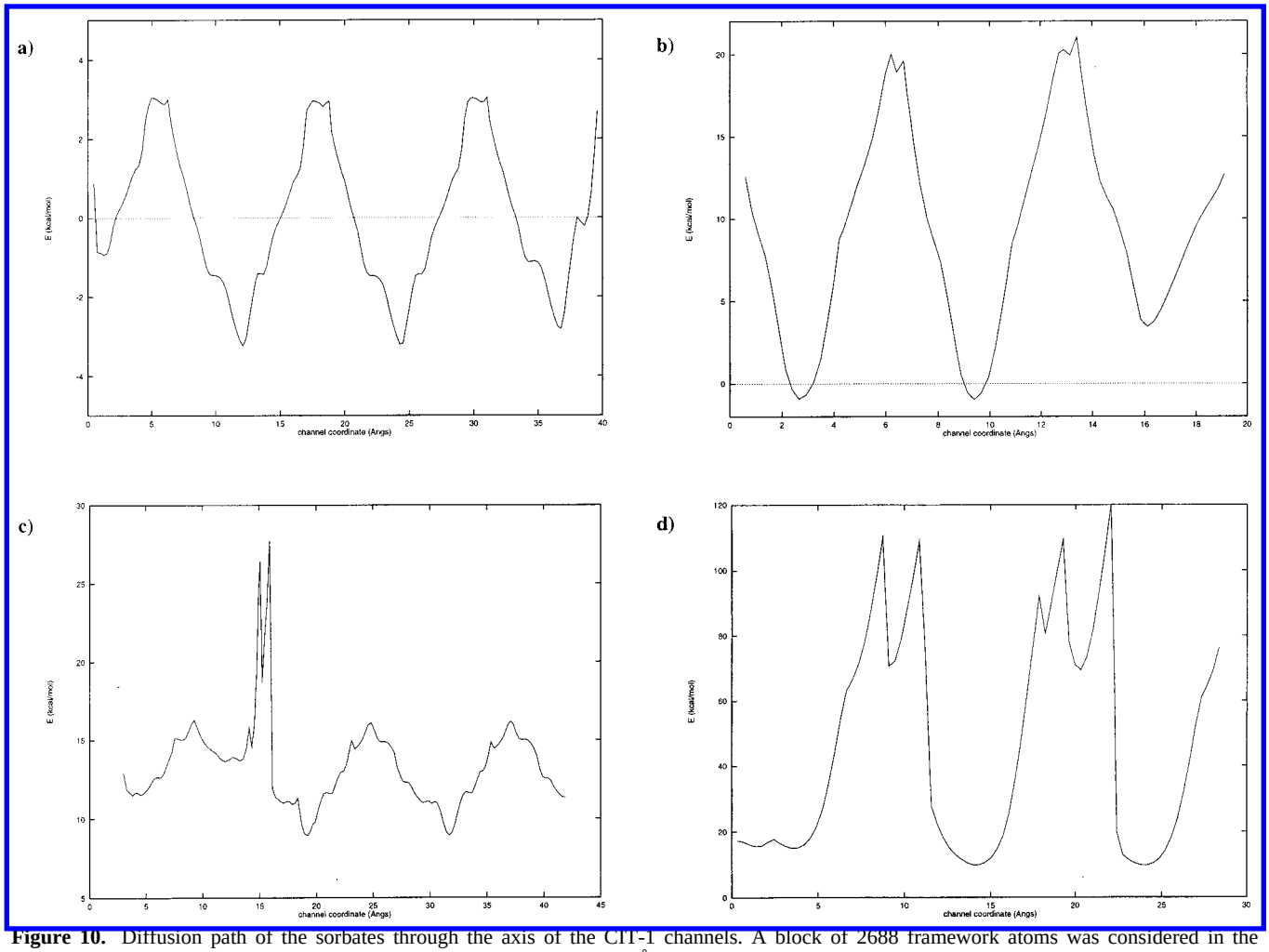

Figure 10. Diffusion path of the sorbates through the axis of the CIT-1 channels. A block of 2688 framework atoms was considered in the simulation. The sorbate was pulled through the channel in steps of 0.2 Å and its position optimized every step. BIOSYM/MSI potentials were used.[36] (a) *p*-xylene through 12 MR channels; (b) *p*-xylene through the 10 MR channels; (c) *o*-xylene through 12 MR channels; d) ortho-xylene through the 10 MR channels.

TABLE 5: Calculated Activation Energies of Xylenes in the Different Channel Systems in CIT-1

xylene and channel system	activation energy (kcal/mol)
p-xylene in 12 MR	6.21
p-xylene in 10 MR	20.93
o-xylene in 12 MR	7.03
o-xylene in 10 MR	110.31

TABLE 6: Experimental Diffusion Coefficients for the Single-Component Diffusion of *p*-Xylene and *o*-xylene in H−CIT-1 Zeolite at Different Temperatures

sorbate	$D \times 10^9$ (cm^2/s)	T (K)
o-xylene	1.3	350
	1.1	375
	1.6	400
	1.0	425
p-xylene	3.7	350
		375
	6.9	400
	15.0	425

silicalite (Table 8). The results show that while the framework composition has a small influence on the values obtained for benzene and toluene, in the case of *m*-xylene a much lower diffusion coefficient is obtained in the Al-containing zeolite, which is due presumably to interaction between the xylene molecules and the Brønsted acid sites. Such effects are likely to be operative in the CIT-1 system studied here. Moreover the presence of extraframework materials in the experimental system could seriously modify the diffusion rate; such effects are of course not included in the MD simulations.

TABLE 7: Diffusional Activation Energy (E_a) and Preexponential Factor from the Relationship $D = D_0 \exp(-E_a/RT)$ for the Single-Component Diffusion of *p*-Xylene and *o*-Xylene in H−CIT-1

sorbate	E_a (kJ/mol)	$D_0 \times 10^4$ (cm^2/s)
p-xylene	10	1.2
o-xylene	33	0.003

In addition, we should also note that the uptake methods used here give results that are lower than those obtained by PFG NMR;[40] indeed, as discussed previously,[8a] only the latter type of microscopic method gives results that are strictly comparable with MD simulations since both are based on the calculation of the mean square displacements (MSD). However, in the case of 10 MR zeolites, even the diffusion of benzene is too slow to be measured by PFG NMR,[17] which would preclude the study of C8 alkylaromatics in CIT-1 by this method.

6. Conclusions

We have found that MD simulation runs of 100 ps for the diffusion of *o*- and *p*-xylene in purely siliceous CIT-1 at 500 K are sufficient to determine the mechanism of diffusion. The variation of the molecular diffusion coefficients with the loading has been investigated through the study of two independent runs with loadings of 1.00 and 0.25 molecule/unit cell, which found

TABLE 8: Values Reported Previously for the Diffusion of Aromatic Hydrocarbons in Zeolites with 10 and 12 MR Channels.

zeolite	sorbate	T (K)	$D \times 10^9$ (cm^2/s)	ref
ZSM-5	benzene	350	3.2	19
ZSM-5	toluene	350	0.9	19
ZSM-5	ethylbenzene	350	1.5	19
ZSM-5	*m*-xylene	350	0.001−0.0001	19
Beta	benzene	350	3.2	19
Beta	ethylbenzene	350	0.2	19
Beta	*m*-xylene	350	0.2	19
Beta	*o*-xylene	350	0.2	19
Na-X	*o*,*m*,*p*-xylene	400	500	38
Na-X	*o*,*m*,*p*-xylene	400	2.5	39
Na-X	*o*,*m*,*p*-xylene	400	2.5	40
silicalite	benzene	373	3.1	41
silicalite	ethylbenzene	373	2.0	41
silicalite	*p*-xylene	373	2.9	41
silicalite	*o*-xylene	373	1.2	41
silicalite	benzene	373	1.1	42
ZSM-5	toluene	320	1.1	43
ZSM-5	toluene	320	0.4	43
ZSM-5	toluene	320	0.6	43

changes from 3.56×10^{-6} cm^2/s to 7.79×10^{-6} cm^2/s, showing the normal trend of decreasing coefficients with increasing loadings. In both cases the *o*-xylene molecules diffuse through the 12 MR channels, as the 10 MR channels are too small for this isomer. Even in the 12 MR channels, the diffusion has certain steric impediments that cause the diffusion path to be confined into a local part of the framework (referred to as "extensive local motion"), normally at the intersection of the two channel systems, where more space is available. Diffusion for the *p*-xylene isomer is much faster, as shown by the calculated diffusion coefficient of 25.2×10^{-6} cm^2/s. On this occasion 12 MR and 10 MR channel systems are utilized, although diffusion takes place more readily through the 12 MR system. The diffusion of *p*-xylene through the 10 MR channels is comparatively much more restricted. The incursions in the 10 MR channels are shorter in time than in the 12 MR channels because the narrower size of the former precludes rotation of the *p*-xylene molecules.

Experimental studies of diffusion of *o*- and *p*-xylene by FTIR yield diffusion coefficients that are about 3 orders of magnitude lower than those obtained in the MD simulations. The reason for this discrepancy can be found in the fact that the uptake methods such as FTIR do not measure the self-diffusivity, which is the quantity found in the MD simulations, and the effects of framework Al and of extraframework material on the observed diffusivity could be appreciable. The use of PFG NMR would give self-diffusivity measurements, but the diffusion seems too slow to be measured by this technique. We also anticipate effects of the loadings of *o*- and *p*-xylene, which will be investigated in future experiments and simulations. For example, higher loadings will increase the proportion of molecules in 10 MR channels in a purely *p*-xylene system, while for an *o*-xylene sample the diffusion will remain confined to the 12 MR channels exclusively. Behavior of mixed "*o*- + *p*-xylene" systems is the subject of further studies currently in progress which will yield a better understanding of the competitive diffusion of both isomers in the mixture.

Acknowledgment. G.S. thanks Ministerio de Educacion y Ciencia of Spain for a postdoctoral research grant. N.R. acknowledges the High Performance Computing Initiative of EPSRC for financial support. We thank Dr. T. R. Forester and Dr. W. Smith for useful discussions and for supplying the DL_POLY code. The EPCC (Edinburgh Parallel Computer Centre) and CRAY-T3D Materials Chemistry Consortium are gratefully acknowledged. We are grateful to Prof. M. E. Davis for providing the sample of CIT-1.

References and Notes

(1) Ruthven, D. M. In *Zeolites: A Refined Tool for Designing Catalytic Sites*; Bonneviot, L., Kaliaguine, S., Eds.; Elsevier Science B. V.: New York, 1995; p 223.
(2) Rabo, J. In *Zeolite Chemistry and Catalysis*; ACS Monograph Series 171; 1976, p 692.
(3) Bullow, M.; Struve, P. *J. Chem. Soc., Faraday Trans. 1* **1984**, *80*, 813.
(4) Barrer, R. M. In *Zeolites and Clay Minerals*, Academic Press: London, 1978, p 299.
(5) Csicsery, S. M. *Zeolites* **1984**, *4*, 202.
(6) Chen, N. Y.; Garwood, W. E.; Dwyer, F. G. In *Shape Selective Catalysis in Industrial Applications*; Dekker: New York, 1989.
(7) Santilli, D. S.; Harris, T. V.; Zones, S. I. *Microporous Mater.* **1993**, *1*, 329.
(8) (a) Nicholas, J. B.; Trouw, F. R.; Mertz, J. E.; Iton, L. E.; Hopfinger, A. J. *J. Phys. Chem.* **1993**, *97*, 4149. (b) Klein, H.; Fuess, H.; Schrimpf, G. *J. Phys. Chem.* **1996**, *100*, 11101.
(9) Karger, J.; Caro, J. *J. Chem. Soc., Faraday Trans. 1* **1977**, 1363.
(10) Jobic, H.; Bee, M.; Caro, J.; Bulow, M.; Karger, J. *J. Chem. Soc., Faraday Trans.* **1989**, *85*, 4201.
(11) Hernandez, E. Ph.D. Thesis, University College, London, 1993.
(12) Demontis, P. Fois, E. S.; Suffriti, G. B.; Quartieri, S. *J. Phys. Chem.* **1990**, *94*, 4329.
(13) Catlow, C. R. A.; Freeman, C. M.; Vessal, B.; Tomlinson, S. M.; Leslie, M. *J. Chem. Soc., Faraday Trans.* **1991**, *87*, 1947.
(14) June, R. J.; Bell, A. T.; Theodorou, D. N. *J. Phys. Chem.* **1992**, *96*, 1051.
(15) Yashonath, S.; Thomas, J. M.; Nowak, A. K.; Cheetham, A. K. *Nature* (*London*), **1988**, *331*, 601.
(16) Hernandez, E.; Kawano, M.; Shubin, A. A.; Freeman, C. M.; Catlow, C. R. A.; Thomas, J. M.; Zamaraev, K. I. In *Proceedings of the 9th International Zeolite Conference*; von Ballmoos, R., Higgins, J. B., Treacy, M. M. J., Eds.; Butterworth-Heinemann: Boston, 1993, p 695.
(17) Karger, J.; Ruthven, D. M. *Diffusion in Zeolites*; John Wiley & Sons: New York, 1992.
(18) Lobo, R. F.; Davis, M. E. *J. Am. Chem. Soc.* **1995**, *117*, 3766.
(19) Roque-Malherbe, R.; Wendelbo, R.; Mifsud, A.; Corma, A. *J. Phys. Chem.* **1995**, *99*, 14064.
(20) Shen, D.; Rees, L. V. C. In *Zeolites: A Refined Tool for Designing Catalytic Sites*; Bonneviot, L., Kaliaguine, S., Eds.; Elsevier Science B. V.: New York, 1995, p 235.
(21) Niessen, W.; Karge, H. *Microporous Mater.* **1993**, *1*, 1.
(22) Klein, H.; Kirschhok, C.; Fuess, H. *J. Phys. Chem.* **1994**, *98*, 12345.
(23) *DL_POLY_2.0 User Manual*; Forester, T. R.; Smith, W. CCLRC Daresbury Laboratory, 1995.
(24) Verlet, L. *Phys. Rev.* **1967**, *159*, 98.
(25) Shannon, D. F. *Math. Comput.* **1970**, *24*, 647.
(26) Gale, J. D. *J. Chem. Soc., Faraday Trans.* **1997**, *93* (*4*), 629.
(27) Schrimpf, G.; Schlenkrich, M.; Brickmann, J.; Bopp, P. *J. Phys. Chem.* **1992**, *96*, 7404.
(28) Allen, M. P.; Tildesley, D. *Molecular Simulation of Liquids*; Oxford University Press: New York, 1980.
(29) Oie, T.; Maggiora, T. M.; Christoffersen, R. E.; Duchamp, D. J. *Int. J. Quantum Chem., Quantum Biol. Symp.* **1981**, *8*, 1.
(30) (a) Auerbach, S. M.; Henson, N. J.; Cheetham, A. K.; Metiu, H. I. *J. Phys. Chem.* **1995**, *99*, 10600. (b) Henson, N. J. Private communication.
(31) Cranck, J. *The Mathematics of Diffusion*; Clarendon: Oxford, 1975.
(32) Rabdel, A.; Sastre, G.; Lewis, D. W.; Catlow, C. R. A. *J. Mater. Chem.* **1996**, *6*, 1837.
(33) Deem, M. W.; Newsam, J. M.; Creighton, J. A. *J. Am. Chem. Soc.* **1992**, *114*, 7198.
(34) Kaeding, W. W.; Chu, C.; Young, L. B.; Butter, S. A. *J. Catal.* **1981**, *69*, 392.
(35) Wei, J. *J. Catal.* **1982**, *76*, 433.
(36) *Catalysis 6.0.0 Software Package*; Biosym/MSI: San Diego, 1995.
(37) Ruthven, D. M.; Eic, M.; Richard, E. *Zeolites* **1991**, *11*, 647.
(38) (a) Goddard, M.; Ruthven, D. M. *Zeolites* **1986**, *6*, 275. (b) Goddard, M.; Ruthven, D. M. *Zeolites* **1986**, *6*, 283.
(39) Eic, M.; Ruthven, D. M. *Zeolites* **1988**, *8*, 258.
(40) Ruthven, D. M.; Eic, E. *Am. Chem. Soc., Symp. Ser.* **1988**, *388*, 362.
(41) Shen, D.; Rees, L. V. C. *Zeolites* **1991**, *11*, 666.
(42) Muller, G.; Narbeshuber, T.; Mirth, G.; Lercher, J. A. *J. Phys. Chem.* **1994**, *98*, 7436.
(43) Germanus, A.; Karger, J.; Pfeiffer, H.; Samulevich, N.; Zhdanov, S. P. *Zeolites* **1985**, *5*, 91.